Supporting information

Effects of Stokes Shift and Purcell Enhancement in Fluorescence-Assisted Radiative Cooling

Xue Ma,[a] Yang Fu,[a] Arsenii Portniagin,[a] Ning Yang,[b] Danjun Liu,[a] Andrey L. Rogach,[a] Jian-Guo Dai,[b] and Dangyuan Lei*[a]

[a] Department of Materials Science and Engineering, The Hong Kong Institute of Clean Energy, and Centre for Functional Photonics (CFP), City University of Hong Kong, 83 Tat Chee Avenue, Kowloon, Hong Kong, 999077, China.

[b] Department of Civil and Environmental Engineering, The Hong Kong Polytechnic University, Hung Hom, Kowloon, Hong Kong, 999077, China.

*Corresponding author

E-mail: dangylei@cityu.edu.hk (D. Y. Lei)

Calculation and simulation

COMSOL simulation of the TiO_2 NP scattering

Numerical simulations of scattering for TiO_2 NPs were conducted using finite-element-method based software COMSOL. Each TiO_2 NPs in Fig. 2 were reproduced in COMSOL with extracted shapes and sizes from zoom-in SEM image. A glass substrate under the NPs and air above the NPs were added in the simulation structures. Periodic boundary conditions and two ports were applied. The refractive index of TiO_2 and glass used in simulation are given in Fig. S1a and S1b. The reproduced structures for TiO_2 NPs in COMSOL were demonstrated in Fig. S1c.

Scattering efficiency of TiO_2 NPs in different dielectric environments

Moreover, the DFS measurement presents typical scattering characteristic of TiO_2 NPs on a glass substrate. However, after added into the coating, dielectric environment will change and influence the scattering spectra. To evaluate the impact of coating, we calculate the scattering efficiency of a spherical TiO_2 NP at diameter of 212 nm, which is approximately the geometry of the TiO_2 NP in Fig. 2d. As shown in Fig. S2, with surrounding medium of air, the peak scattering exhibits red shift than DFS result due to the low refractive index of air. While with surrounding medium of the coating, blue shift emerges for peak scattering. Therefore, BAM with shorter emission peak will match the scattering peak of TiO_2 NPs in the coating better than S541.

Theoretical solar reflectance through Monte Carlo calculations

To understand the influence of different fillers on solar reflectance of the coatings, we performed Monte Carlo calculations based on random particles distribution.[1-3] TiO_2 NPs were assumed to be spherical to obtain analytical solutions for their scattering parameters. Three coatings (matrix + TiO_2 NPs; matrix + hollow glass spheres; and matrix + TiO_2 NPs + hollow glass spheres) were calculated and analyzed as shown in Fig. S6. The size distributions and volume fractions of the fillers are given in Fig. S3a, Fig. S5b and Table. S2. It can be observed that the solar reflectance of the coatings is benefited mainly from TiO_2 NPs rather than from hollow glass spheres. Hollow glass spheres will not influence the overall solar reflectance since their sizes are too large to produce Mie resonances and thereby manifest low scattering efficiency.

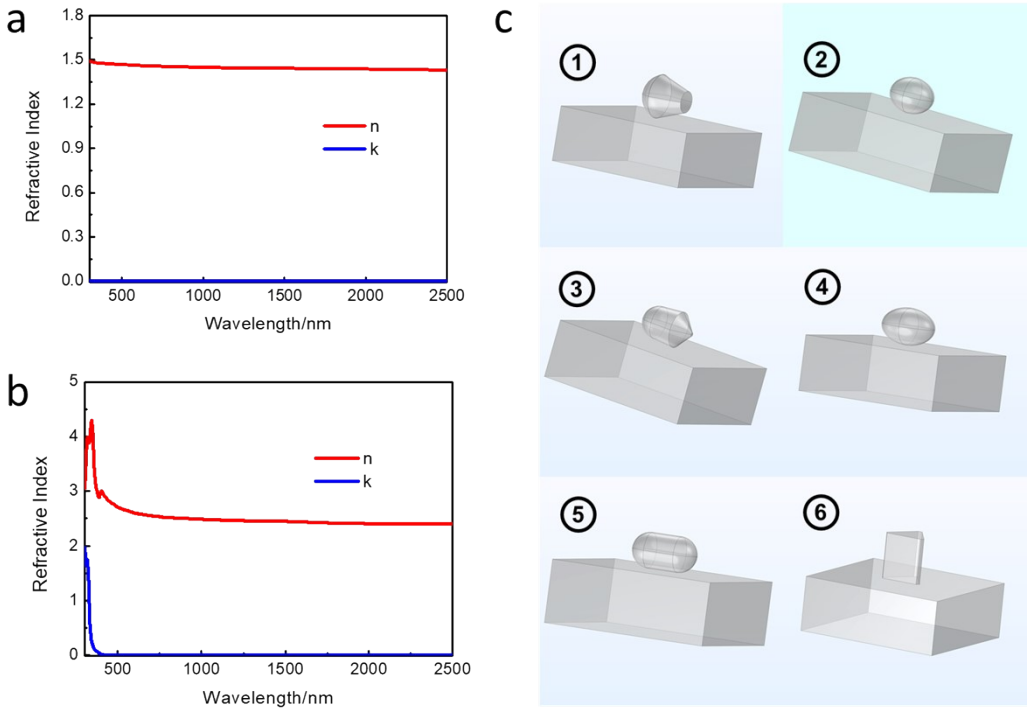

Fig. S1 Refractive index of (a) the glass substrate and (b) TiO_2 NPs in simulation. (c) Structures on glass substrates built in COMSOL for six single particles in Figure 2.

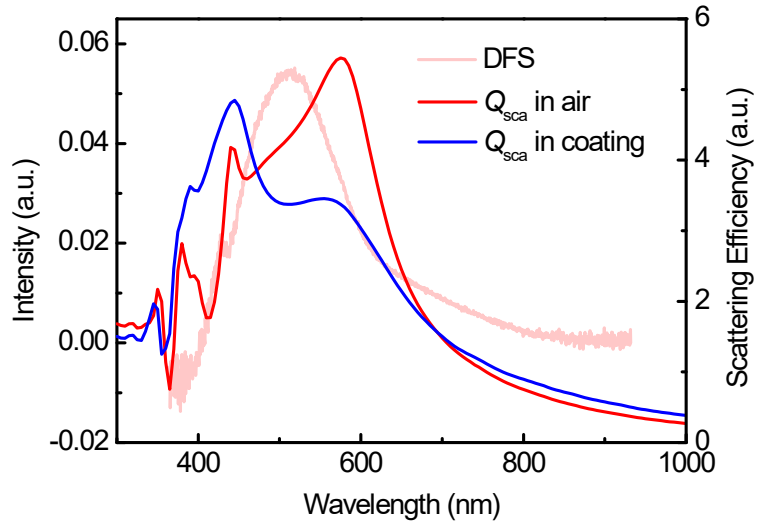

Fig. S2 DFS spectra of TiO_2 NP in Fig. 2d (pink) and calculated scattering efficiency of spherical TiO_2 NP at diameter of 212 nm in air (red) and in coating (blue). Blue shift of scattering peaks can be observed for TiO_2 NP in coating.

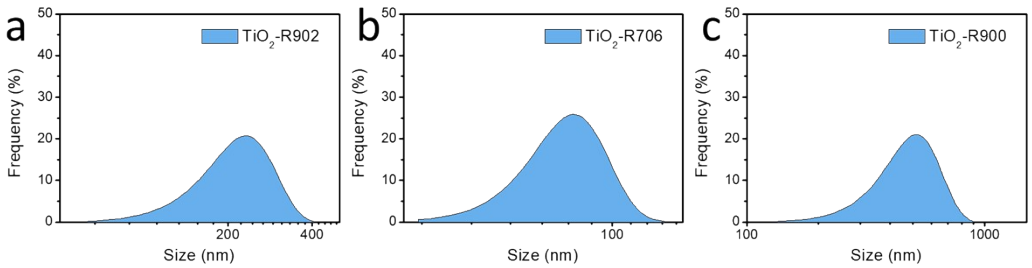

Fig. S3 Size distributions of TiO_2 powders with model of (a) R902, (b) R706 and (c) R900, respectively. R902 is chosen for cooling coating preparation and DFS measurement in this work.

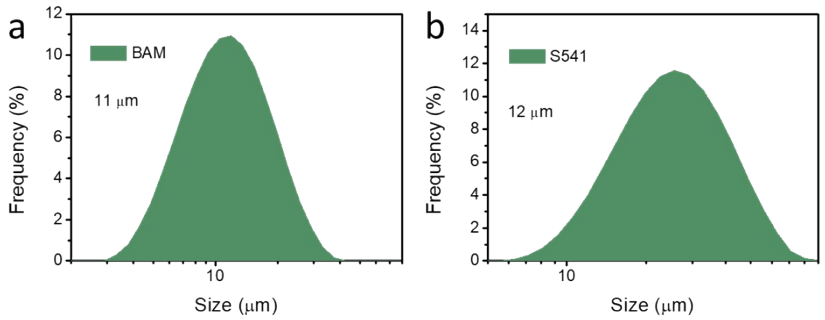

Fig. S4 Size distribution of (a) BAM phosphor and (b) S541 phosphor.

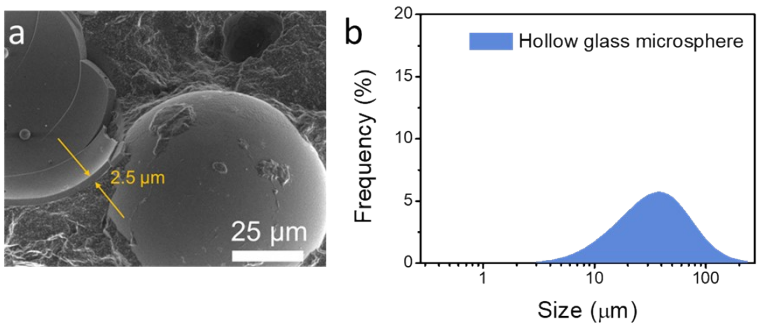

Fig. S5 (a) Cross-section SEM image of a hollow glass microsphere. The shell thickness is fixed at ~2.5 μm. (b) Size (outer diameter) distribution of hollow glass microspheres.

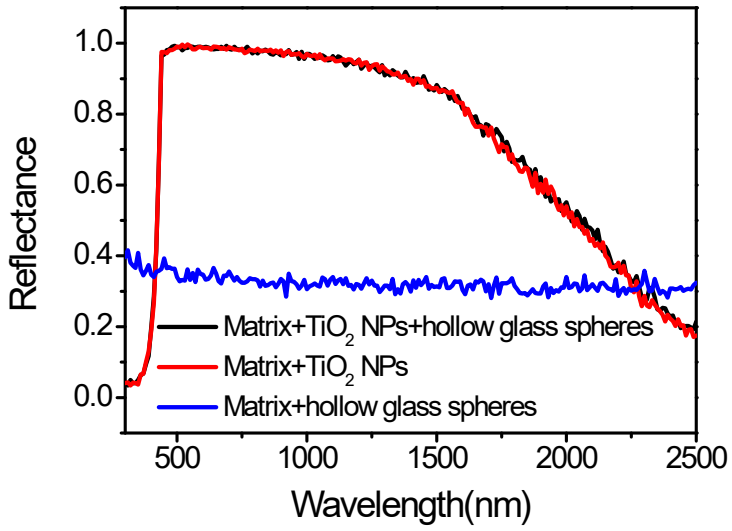

Fig. S6 Theoretical solar reflectance of three different coatings based on Monte Carlo calculations.

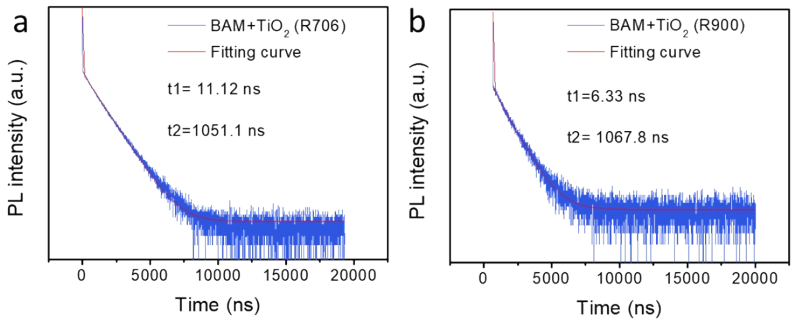

Fig. S7 PL lifetime of BAM phosphor after added in cooling coating based on (a) R706 TiO_2 and (b) R900 TiO_2, respectively.

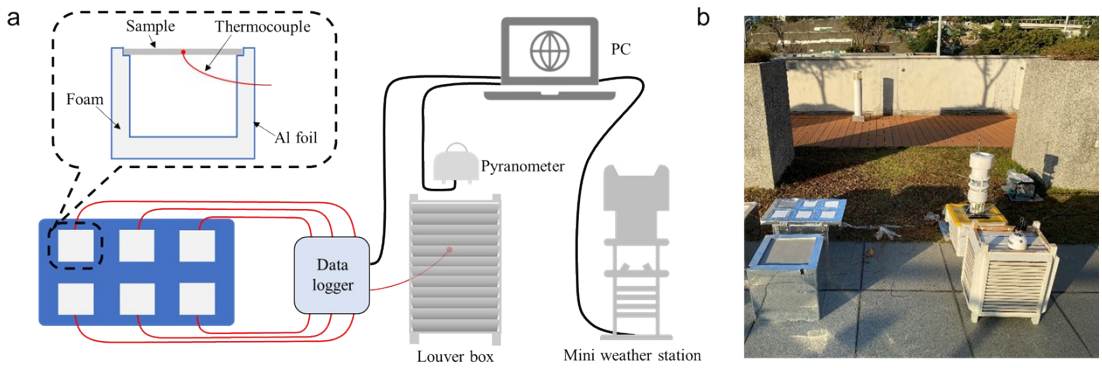

Fig. S8 Schematics and a photograph of the apparatus used for the field test.

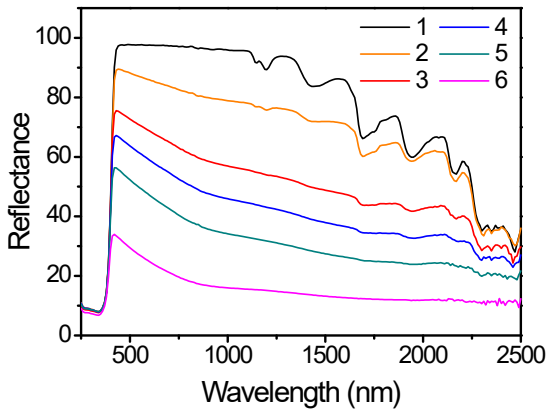

Fig. S9 Reflectance of six reference coatings mixing with different amount of black pigment.

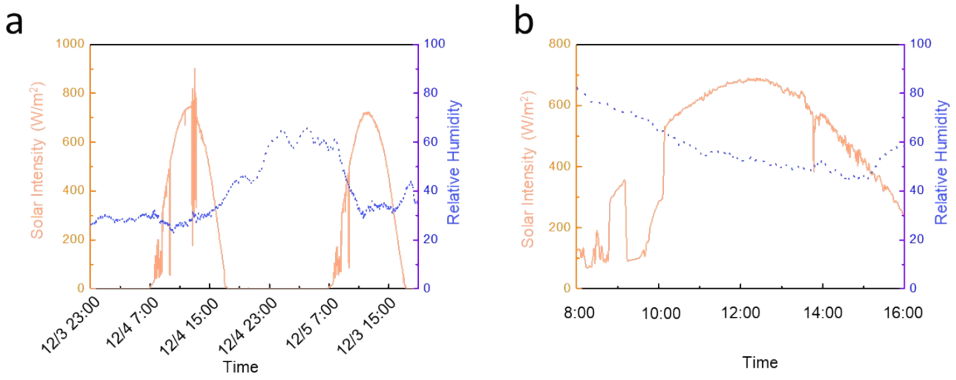

Fig. S10 Solar intensity and relative humidity in field tests for (a) Figure 3a-3b, (b) Figure 3c-3d and Figure 4b. The peak solar intensity (~700 W/m^2) in (b) was used for cooling power calculation in Figure 4d.

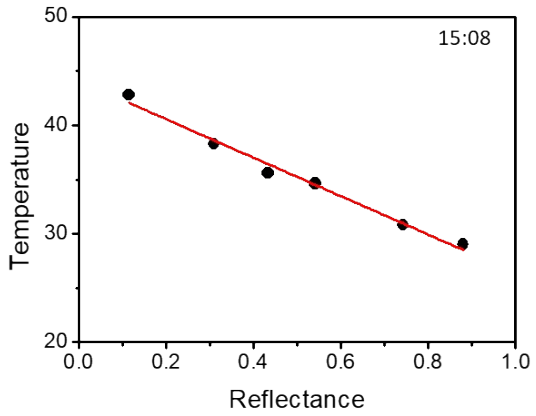

Fig. S11 Temperature fitting of reference samples. The temperature of reference coatings varies nearly linearly with total solar reflectance.

Table S1 Fitted radiative lifetime (τ_2) and non-radiative lifetime (τ_1) for pure phosphors and phosphors in cooling coating.

Sample	τ_1 (ns)	τ_2 (ns)
Pure BAM	387	1152
BAM-2g in coating	11	446
Pure S541	264	819
S541-2g in coating	177	627

Table S2 Densities, weights and volume fractions of main components in fluorescent and white coatings.

Component	Density (g/cm^3)	Weight (g) in fluorescent coating	Volume fraction (%) in fluorescent coating	Weight (g) in white coating	Volume fraction (%) in white coating
Polymer matrix (dried)	0.85	10	43.0	10	44.2
TiO_2 NPs	4.23	12	10.4	12	10.7
Fluorescent microparticles (BAM)	3.44	2	2.8	0	0
Hollow glass spheres	0.25	3	43.8	3	45.1

Table S3 Measured solar reflectance for six reference coatings.

Reference sample No.	UV reflectance	Visible reflectance	Near-infrared reflectance	Solar reflectance
1	0.0968	0.9258	0.8946	0.8796
2	0.0973	0.7868	0.7488	0.7426
3	0.0938	0.5800	0.5378	0.5412
4	0.0957	0.4609	0.4318	0.4331
5	0.0962	0.3149	0.3194	0.3089
6	0.0843	0.0817	0.1487	0.1145

Table S4 Fitted ESR for six fluorescent cooling coatings in Figure 4d.

Time	BAM-2g	BAM-4g	BAM-6g	S541-2g	S541-4g	S541-6g
11:23	0.8835	0.8133	0.8002	0.8440	0.8440	0.8309
11:56	0.9052	0.8318	0.8202	0.8665	0.8704	0.8511
12:32	0.8842	0.8199	0.8123	0.8502	0.8539	0.8426
12:55	0.8920	0.8274	0.8202	0.8561	0.8597	0.8489
13:13	0.8998	0.8362	0.8100	0.8586	0.8736	0.8474
13:43	0.8958	0.8352	0.8069	0.8554	0.8635	0.8433
14:16	0.9148	0.8327	0.8154	0.8543	0.8673	0.8413
14:51	0.8964	0.8327	0.8284	0.8582	0.8624	0.8454
15:08	0.9198	0.8140	0.7973	0.8363	0.8418	0.8251

Table S5 Comparison of fluorescent pigments used in this work and previous study (Ref. 24).

Phosphor	BAM	S541	$SrAl_2O_4:Eu^{2+},Dy^{3+},Yb^{3+}$ (Ref. 24)
Excitation peak (nm)	333	341	420
Emission peak (nm)	463	539	525
Stokes shift (nm)	130	198	105
Quantum yield (%)	90	90	64
Purcell factor	2.6	1.3	1.4
Max ESR improvement (%)	4	-1%	3.6%

References:

1. Peoples, J., Li, X., Lv, Y., Qiu, J., Huang, Z., & Ruan, X. (2019). A strategy of hierarchical particle sizes in nanoparticle composite for enhancing solar reflection. International Journal of Heat and Mass Transfer, 131, 487-494.

2. Yalçın, R. A., Blandre, E., Joulain, K., & Drévillon, J. (2020). Colored radiative cooling coatings with nanoparticles. ACS Photonics, 7(5), 1312-1322.

3. Fu, Y., An, Y., Xu, Y., Dai, J. G., & Lei, D. (2022). Polymer coating with gradient-dispersed dielectric nanoparticles for enhanced daytime radiative cooling. EcoMat, 4(2), e12169.